



TOTAL IONIZING DOSE TEST REPORT

No. 03T-RT54SX32S-T25JS003

May 5, 2003

J.J. Wang
(408) 522-4576
jih-jong.wang@actel.com

I. SUMMARY TABLE

Parameter	Tolerance
1. Gross Functionality	Passed 100 krad(Si)
2. I _{CC}	Passed 66 krad(Si) on 25 mA spec, I _{CC} is averaging 85 mA after 100 krad(Si) and room temp annealing
3. Input Threshold (V _{TIL} /V _{IH})	Passed 100 krad(Si)
4. Output Drives (V _{OL} /V _{OH})	Passed 100 krad(Si)
5. Propagation Delays	Passed 88.7 krad(Si) on 10% degradation, less than 13% degradation after 100 krad(Si)
6. Transition Time	Passed 100 krad(Si)

II. TOTAL IONIZING DOSE (TID) TESTING

A. Device Under Test (DUT) and Irradiation

Table 1 lists the DUT information and irradiation conditions.

Table 1. DUT information and irradiation conditions

Part Number	RT54SX32S
Package	CQFP256
Foundry	Matsushita Electronics Corporation
Technology	0.25 μ m CMOS
DUT Design	TDSX32CQFP256_2Strings
Die Lot Number	T25JS003
Quantity Tested	5
Serial Number	13503, 13529, 13545, 13611, 13615
Radiation Facility	Defense Microelectronics Activity
Radiation Source	Co-60
Dose Rate	1 krad(Si)/min ($\pm 5\%$)
Irradiation Temperature	Room
Irradiation and Measurement Bias (V _{CC1} /V _{CCA})	Static at 5.0 V/2.5 V

B. Test Method

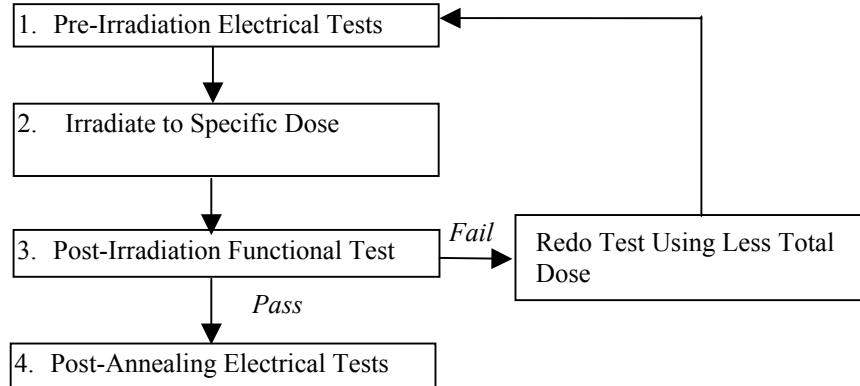


Fig 1 Parametric test flow chart

The parametric tests follow the military standard test method 1019.5. Fig 1 shows the testing flow. The time dependent effect (TDE) of this product was previously evaluated by comparing the results of a high dose rate (1 krad(Si)/min) against the results of a low dose rate (1 krad(Si)/hr). No adverse TDE was observed. Therefore the accelerated aging test (rebound test) is omitted. Room temperature annealing were performed for 3 weeks after 100 krad(Si) of irradiation. Every DUT was static biased during annealing except DUT 13615, which was dynamically annealed for one day during the 3-week annealing period. As will be shown in the following sections, the post-annealed I_{CC} and propagation delay of DUT 13615 are significantly less than those of any other DUT. The reason is that the dynamic operation elevated the device temperature and enhanced the annealing effects. It indicates that the post accelerated aging test would show better results than those shown by post room temperature annealing test.

C. Electrical Parameter Measurements

A high utilization design (TDSX32CQ256_2Strings) to address total dose effects in typical space applications is used. The circuit schematics are shown in appendix A.

Table 2 lists the electrical parameters measured. The functionality is measured pre-irradiation, post-irradiation, and post-annealing on the output pin (O_AND3 or O_AND4) of the two combinational buffer-strings and on the output pins (O_OR4 and O_NAND4) of the shift register. I_{CC} is measured on the power supply of the logic-array (I_{CCA}) and I/O (I_{CCI}) respectively.

The input logic thresholds (V_{IL}/V_{IH}) and output drives (V_{OL}/V_{OH}) are measured pre-irradiation and post-annealing on a combinational net, the input pin DA to the output pin QA0. The propagation delays are measured pre-irradiation and post-annealing on the O_AND4 output of one of the buffer strings. The delay is defined as from the input CLOCK to the output. The transient times (rise and fall times) are measured pre-irradiation and post-annealing on the O_AND4 output.

Each unused input is grounded with an 1 M ohm resistor during irradiation and an 1.2K ohm resistor during annealing.

Table 2. Logic design for parametric tests

Parameter/Characteristics	Logic Design
1. Functionality	All key architectural functions (pins O_AND3, O_AND4, O_OR3, O_OR4, and O_NAND4)
2. I_{CC} (I_{CCA}/I_{CCI})	DUT power supply
3. Input Threshold (V_{TIL}/V_{IH})	TTL compatible input buffer (pin DA to QA0)
4. Output Drive (V_{OL}/V_{OH})	TTL compatible output buffer (pin DA to QA0)
5. Propagation Delay	String of buffers (pin LOADIN to O_AND4)
6. Transition Time	D flip-flop output (O_AND4)

III. TEST RESULTS

A. *Functionality*

Every DUT passed the gross functional test at pre-irradiation, post-irradiation, and post-annealing.

B. I_{CC}

Figs 2-6 show the in-flux I_{CC} plots. For the same accumulative total dose, I_{CC} at the present dose rate of 1 krad(Si)/min is significant higher than the results tested at lower dose rate of 1 krad(Si)/hr (see, for example, report No. 02T-RT54SX32S-T25JS001). At 100 krad(Si) total dose, I_{CC} (I_{CCA} and I_{CCI}) for high dose rate is averaging 224.8 mA, while I_{CC} average for low dose rate is less than half of that.

Except DUT 13615, the average I_{CC} dropped to 85 mA after annealing. I_{CC} of DUT 13615 dropped to 53 mA, significantly lower than that of any other DUT because of its dynamic annealing. The radiation tolerance based on the 25 mA spec can to be extracted from the annealing characteristic. Fig 7 shows the annealing characteristic of DUT 13772. The current is normalized with the peak current at 100 krad(Si) total dose. The log-log plot shows a straight line after the short initial stage. Extending the curve to 10 years mission time, the annealing factor is obtained approximately as 0.32 for I_{CCA} and 0.29 for I_{CCI} . These annealing factors are the same values as those measured previously in both RT54SX32S and RT54SX72S, see Fig 6 in report 03T-RT54SX32S-T25JS004 and Fig 7 in 03T-RT54SX72S-T25KS006. Assume that annealing factors are dependent on the product and bias voltage but relatively independent of the total dose in the range of interest, the critical total dose ($\gamma_{critical}$) for the 10-year mission to induce I_{CC} to 25 mA can be obtained by the equation,

$$I_{CCA}(\gamma_{critical}) \times 0.32 + I_{CCI}(\gamma_{critical}) \times 0.29 = 25mA$$

Where $I_{CCA}(\gamma)$ and $I_{CCI}(\gamma)$ are read from the raw data which generates Fig 6. The tolerance ($\gamma_{critical}$) is thus obtained as approximately 66 krad(Si). This number is believed to be overly pessimistic. Theoretically and empirically, the DUT irradiated at high dose rate and then annealed for duration to match the total mission time has significantly higher final I_{CC} than that in a DUT irradiated at a low, uniform dose rate throughout the total mission time.

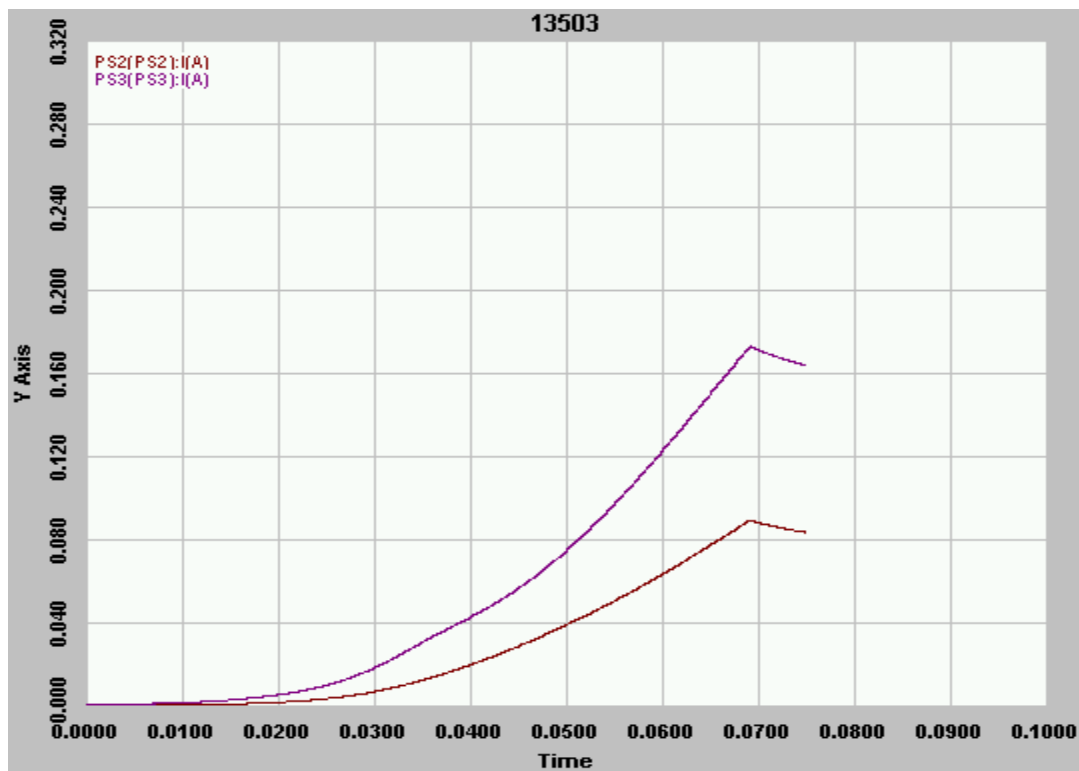


Fig 2 In-flux I_{CC} of DUT 13503, PS2 supplies I_{CCI} and PS3 supplies I_{CCA} . The current unit is amps and the time unit is days, 0.01 day is equivalent to 14.4 krad(Si). I_{CC} reaches the peak at 100 krad(Si), irradiation stops after 100 krad(Si) and I_{CC} drops due to annealing effect.

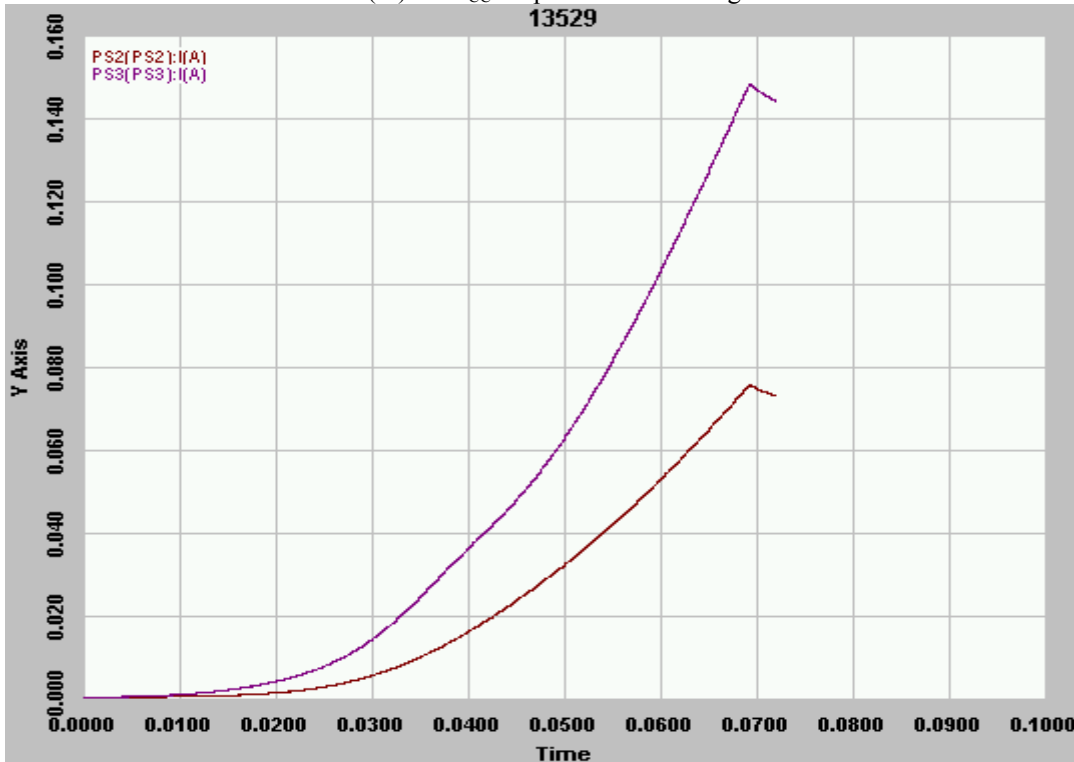


Fig 3 In-flux I_{CC} of DUT 13529, PS2 supplies I_{CCI} and PS3 supplies I_{CCA} . The current unit is amps and the time unit is days, 0.01 day is equivalent to 14.4 krad(Si). I_{CC} reaches the peak at 100 krad(Si), irradiation stops after 100 krad(Si) and I_{CC} drops due to annealing effect.

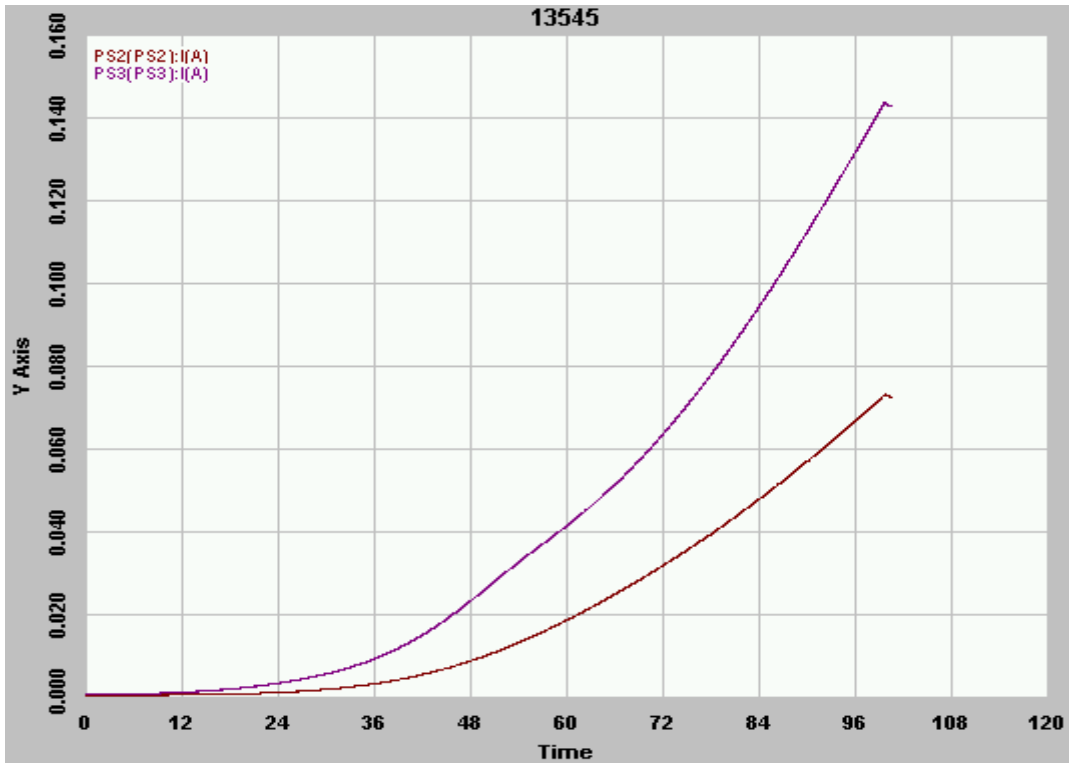


Fig 4 In-flux I_{CC} of DUT 13545, PS2 supplies I_{CCI} and PS3 supplies I_{CCA} . The current unit is amps and the time unit is minutes, 1 min is equivalent to 1 krad(Si). I_{CC} reaches the peak at 100 krad(Si), irradiation stops after 100 krad(Si) and I_{CC} drops due to annealing effect.

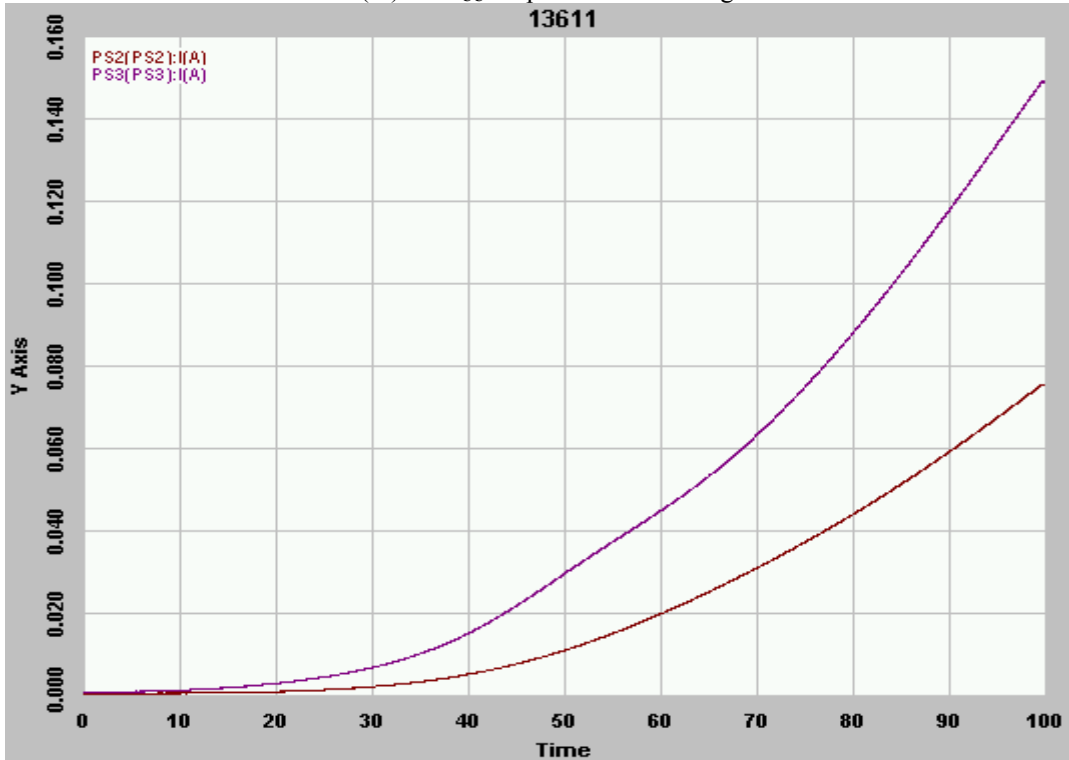


Fig 5 In-flux I_{CC} of DUT 13611, PS2 supplies I_{CCI} and PS3 supplies I_{CCA} . The current unit is amps and the time unit is minutes, 1 min is equivalent to 1 krad(Si). I_{CC} reaches the peak at 100 krad(Si), irradiation stops after 100 krad(Si) and I_{CC} drops due to annealing effect.



Fig 6 In-flux I_{CC} of DUT 13615, PS2 supplies I_{CCI} and PS3 supplies I_{CCA} . The current unit is amps and the time unit is minutes, 1 min is equivalent to 1 krad(Si). I_{CC} reaches the peak at 100 krad(Si), irradiation stops after 100 krad(Si) and I_{CC} drops due to annealing effect.

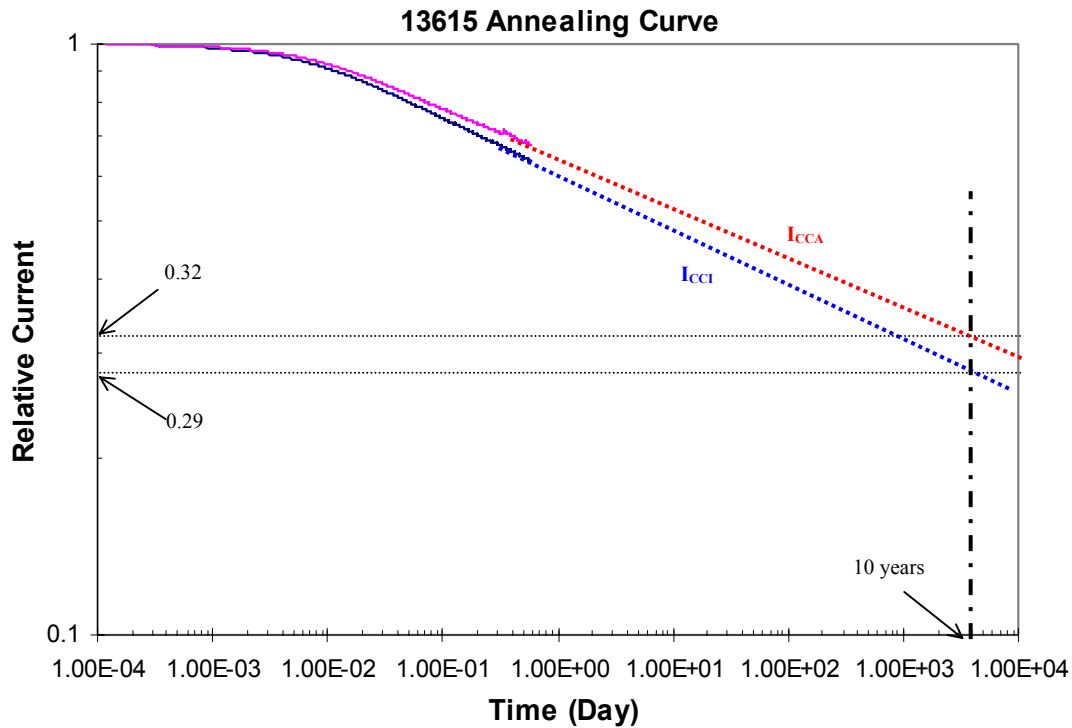


Fig 7 I_{CC} annealing curve, the dotted lines are extrapolations for the 10 years flight mission.

C. Input Logic Threshold (V_{IL}/V_{IH})

Table 4 lists the pre-irradiation and post-annealing input logic threshold for each DUT. All data are well within the spec limits.

Table 4 Pre-irradiation and post-annealing input logic threshold in volts

DUT	Pre-Irradiation		Post-Annealing	
	V_{IL}	V_{IH}	V_{IL}	V_{IH}
13503	1.29	1.51	1.21	1.45
13529	1.31	1.53	1.24	1.48
13545	1.30	1.53	1.24	1.47
13611	1.30	1.52	1.24	1.47
13615	1.35	1.57	1.23	1.47

D. Output Characteristics (V_{OL}/V_{OH})

The pre-irradiation and post-annealing V_{OL}/V_{OH} are listed in table 5 and 6. The post-annealing data are well within the spec limits, and 100 krad(Si) radiation has little effect on these parameters.

Table 5 Pre-irradiation and post-annealing V_{OL} (in volts) at various sinking current

DUT	1 mA		12 mA		20 mA		50 mA		100 mA	
	Pre-rad	Pos-an								
13503	0.008	0.009	0.101	0.101	0.168	0.169	0.425	0.425	0.875	0.874
13529	0.009	0.009	0.104	0.103	0.173	0.172	0.436	0.434	0.898	0.893
13545	0.009	0.009	0.104	0.104	0.173	0.173	0.436	0.436	0.898	0.897
13611	0.009	0.009	0.104	0.105	0.173	0.175	0.434	0.442	0.876	0.909
13615	0.009	0.009	0.104	0.103	0.173	0.172	0.434	0.433	0.904	0.891

Table 6 Pre-irradiation and post-annealing V_{OH} (in volts) at various sourcing current

DUT	1 mA		8 mA		20 mA		50 mA		100 mA	
	Pre-rad	Pos-an								
13503	4.98	4.99	4.87	4.87	4.67	4.67	4.14	4.14	3.08	3.08
13529	4.98	4.98	4.87	4.86	4.66	4.66	4.12	4.11	3.03	3.03
13545	4.98	4.98	4.87	4.87	4.66	4.66	4.13	4.12	3.06	3.06
13611	4.98	4.99	4.87	4.87	4.66	4.66	4.12	4.11	3.04	3.04
13615	4.98	4.98	4.86	4.86	4.66	4.66	4.12	4.11	3.02	3.02

E. Propagation Delays

Tables 7 and 8 list the pre-irradiation and post-annealing propagation delays and radiation-induced degradations. The dynamically annealed DUT 13615 shows less degradation. The worst-case degradation is within 13%. To extract the tolerance of 10% degradation, a piece-wise linear fitting curve of propagation delay against total dose is used. This approach is based on experimental data measured on SXS products. To be conservative, the worst degradation of 12.31% is used. The piece-wise linear fitting curve has two regions, region 1 from 0 krad(Si) to 40 krad(Si) has 0% degradation, and region 2 from 40 krad(Si) to 100 krad(Si) has a slope defined in the equation,

$$\text{Slope} = \frac{\text{TPD}(\text{Max Dose}) - \text{TPD}(\text{Initial})}{\text{Maximum Dose} - 40\text{krad}}$$

Where TPD is measured in percentage. In this case, TPD(Max Dose) is 12.31%, and TPD(Initial) is 0%. The maximum dose is 100 krad(Si). The total dose corresponding to 10% degradation on the linear curve in region 2 is the standard 10% degradation tolerance, which is obtained as 88.7 krad(Si).

Table 7 Low to high delays (in nanoseconds)

DUT	Pre-Irradiation	Post-Anneal	Degradation
13503	436.52	455.11	4.26%
13529	446.47	499.68	11.92%
13545	437.21	489.05	11.86%
13611	439.36	461.62	5.07%
*13615	438.39	453.95	3.55%

*13615 is annealed dynamically

Table 8 High to low delays (in nanoseconds)

DUT	Pre-Irradiation	Post-Anneal	Degradation
13503	359.87	380.82	5.82%
13529	371.59	417.34	12.31%
13545	362.16	405.67	12.01%
13611	362.35	396.42	9.40%
*13615	361.32	376.43	4.18%

*13615 is annealed dynamically

F. Transition Time

The pre-irradiation and post-annealing rising and falling edges are plotted in Figs 8-17. In each case, the radiation-induced degradation is almost invisible, and the transition time both before and after irradiation is always approximately 2 nanoseconds.

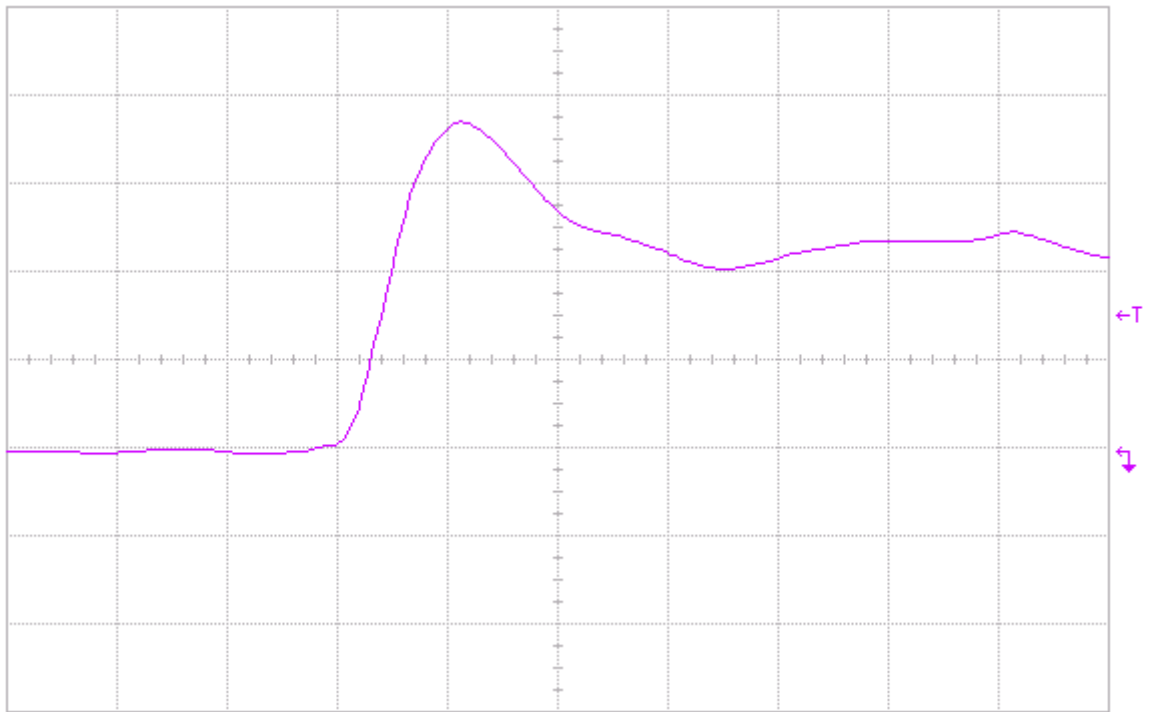


Fig 8(a) Pre-irradiation rising edge of DUT 13503, abscissa scale is 2 V/div and ordinate scale is 2 ns/div.

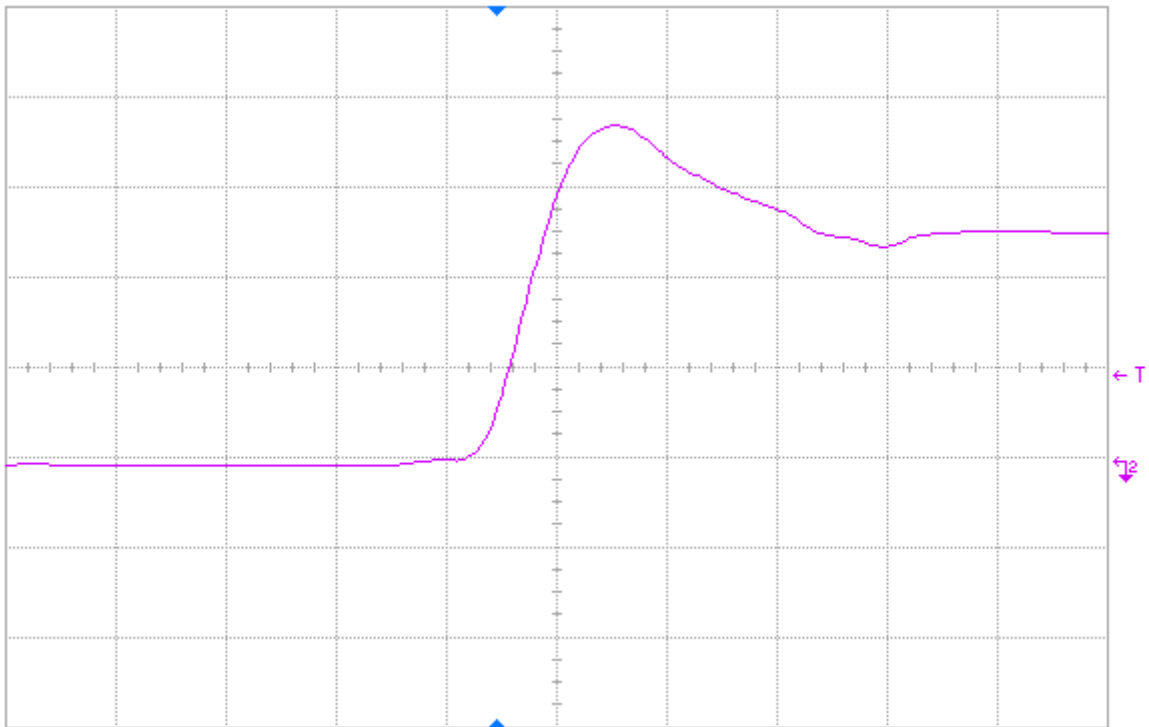


Fig 8(b) Post-annealing rising edge of DUT 13503, abscissa scale is 2 V/div and ordinate scale is 2 ns/div.

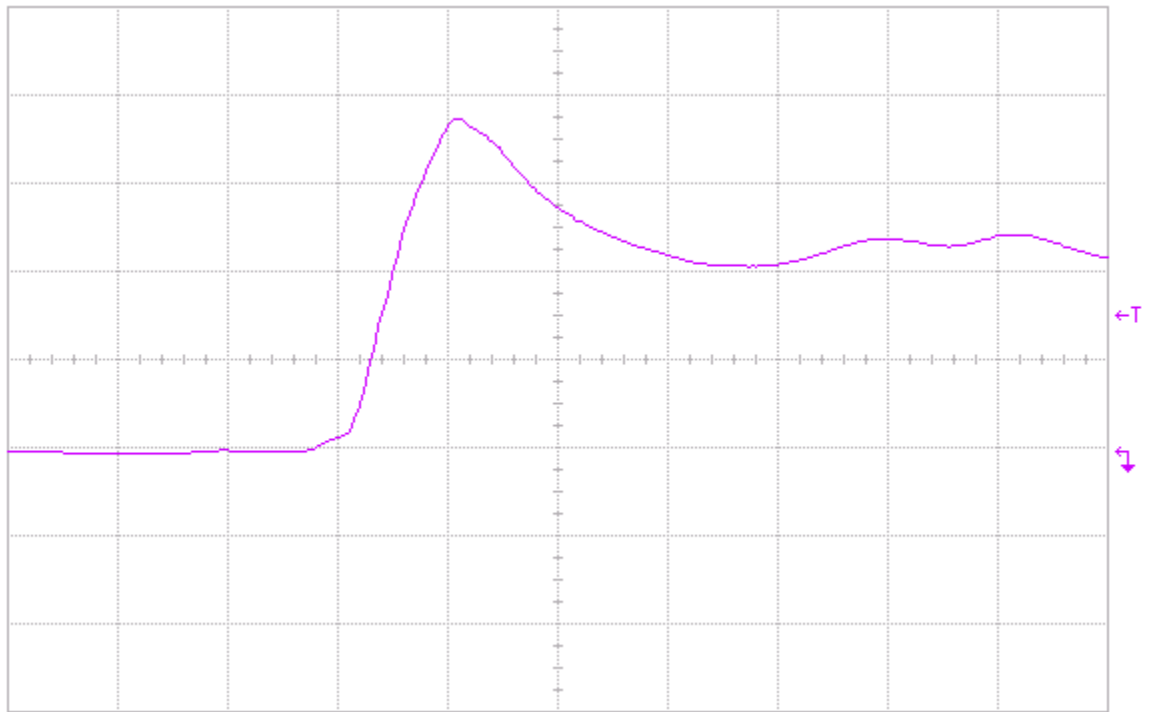


Fig 9(a) Pre-irradiation rising edge of DUT 13529, abscissa scale is 2 V/div and ordinate scale is 2 ns/div.

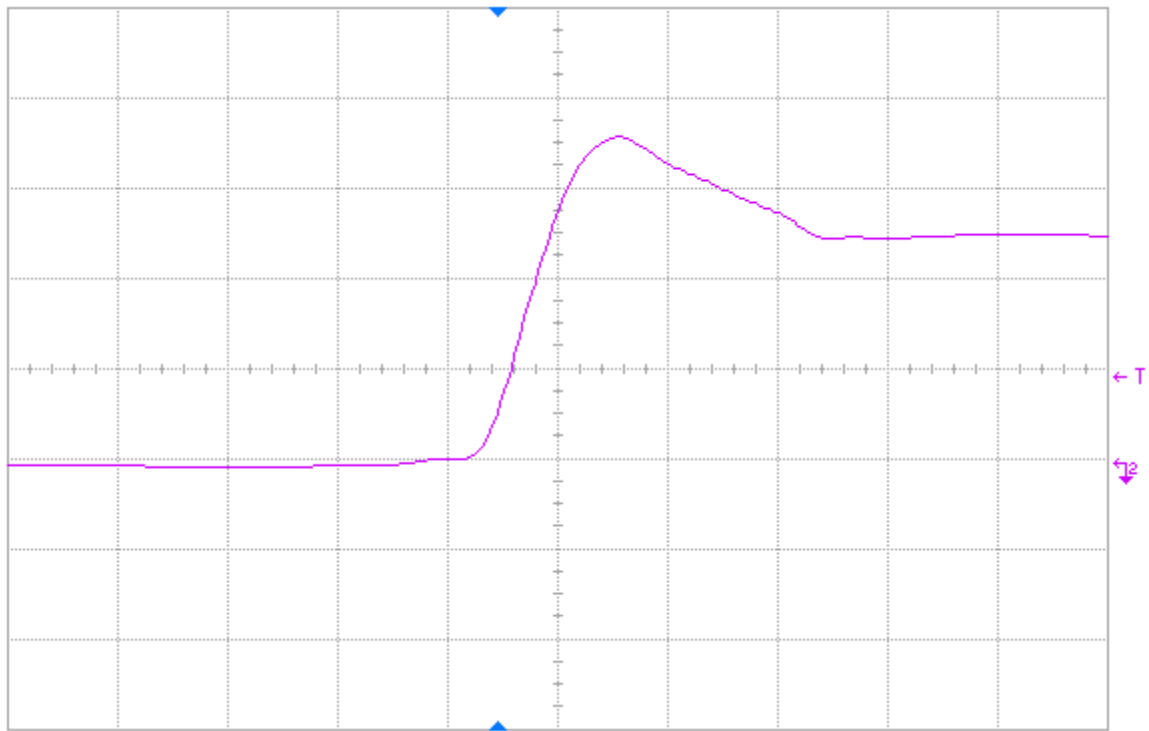


Fig 9(b) Post-annealing rising edge of DUT 13529, abscissa scale is 2 V/div and ordinate scale is 2 ns/div.

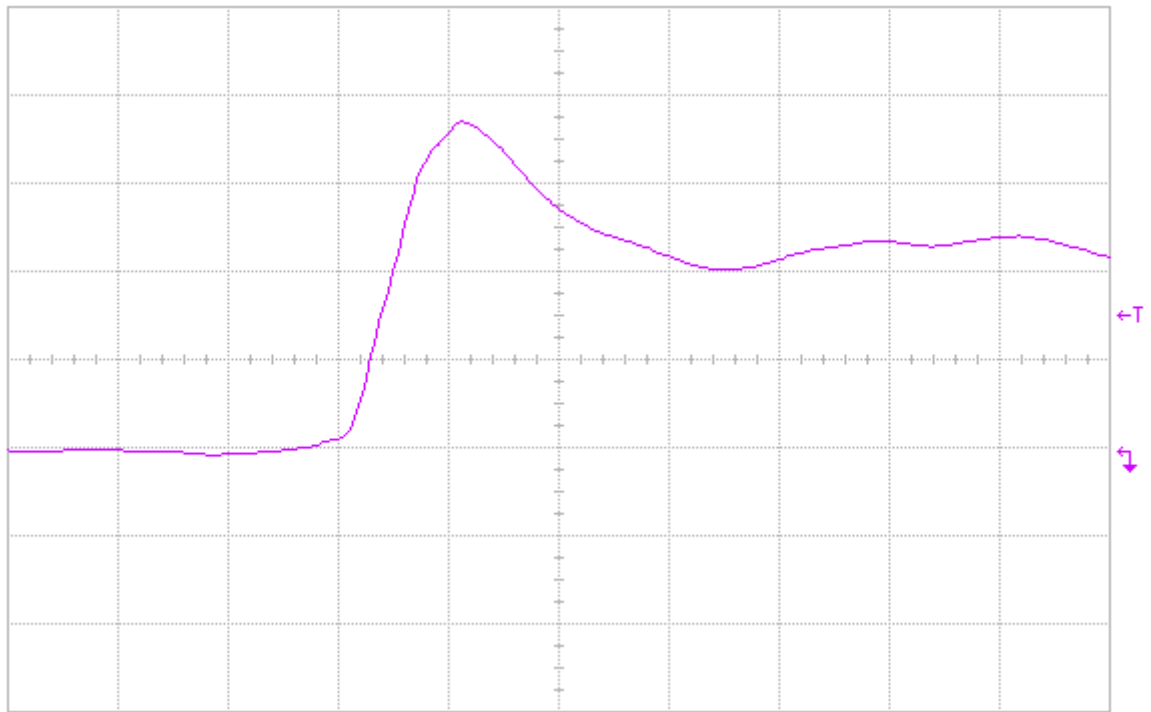


Fig 10(a) Pre-irradiation rising edge of DUT 13545, abscissa scale is 2 V/div and ordinate scale is 2 ns/div.

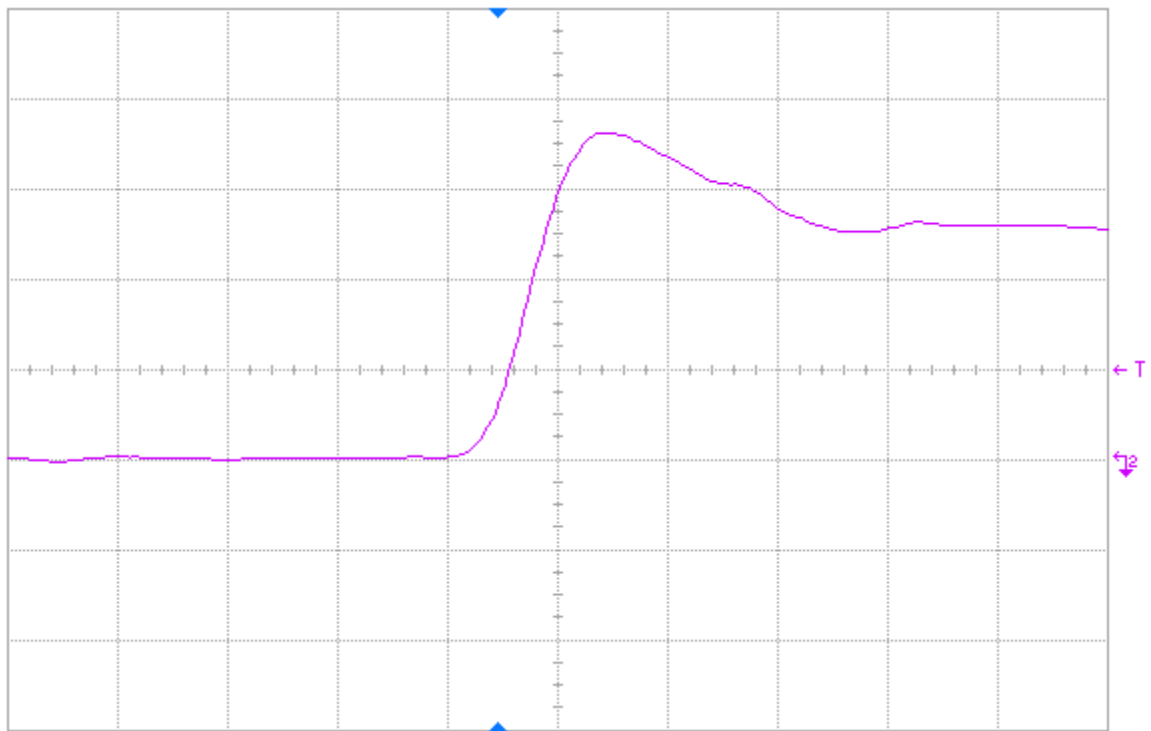


Fig 10(b) Post-annealing rising edge of DUT 13545, abscissa scale is 2 V/div and ordinate scale is 2 ns/div.

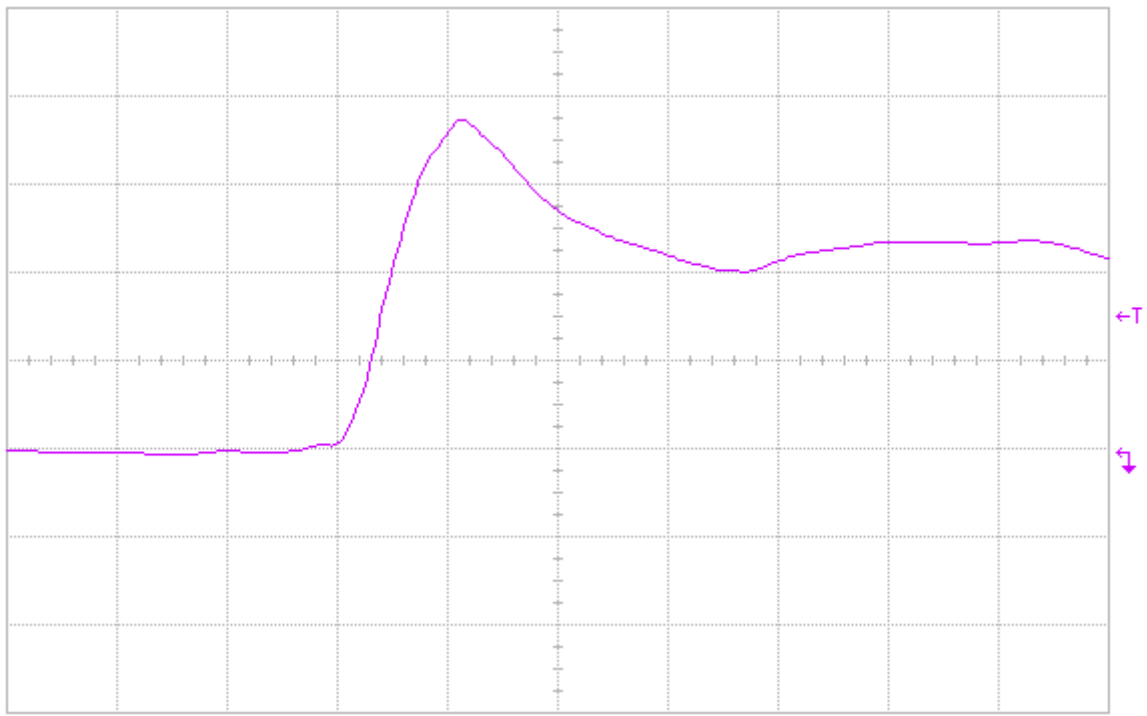


Fig 11(a) Pre-irradiation rising edge of DUT 13611, abscissa scale is 2 V/div and ordinate scale is 2 ns/div.

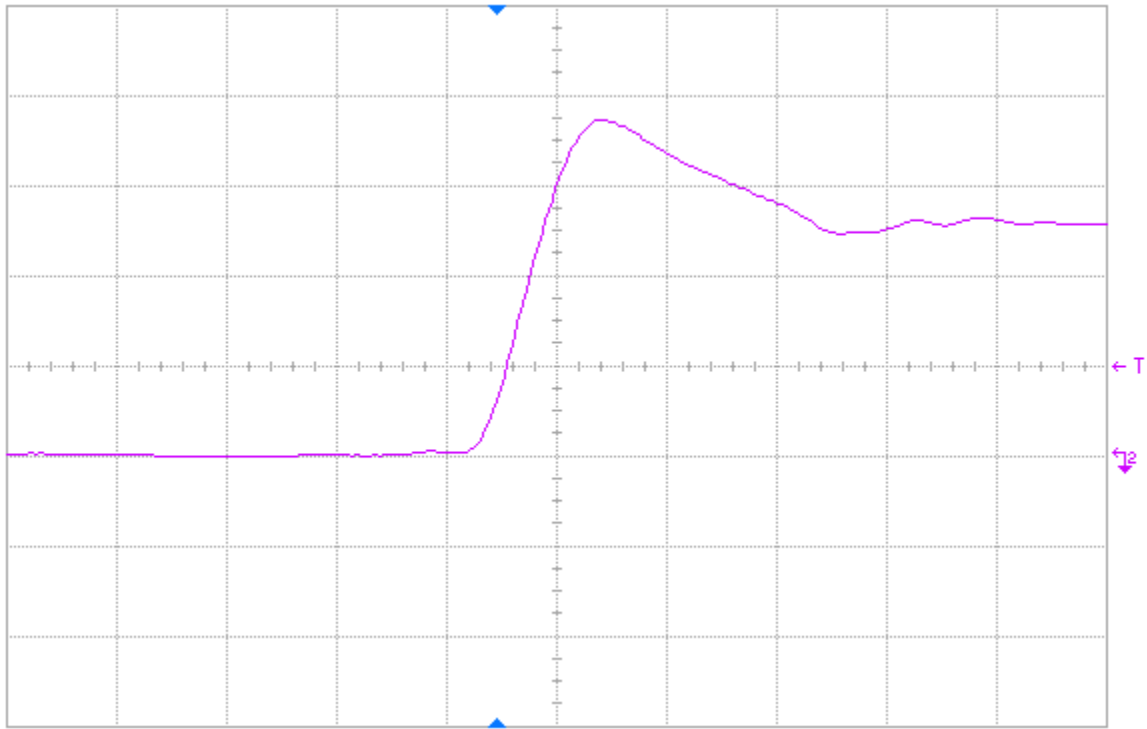


Fig 11(b) Post-annealing rising edge of DUT 13611, abscissa scale is 2 V/div and ordinate scale is 2 ns/div.

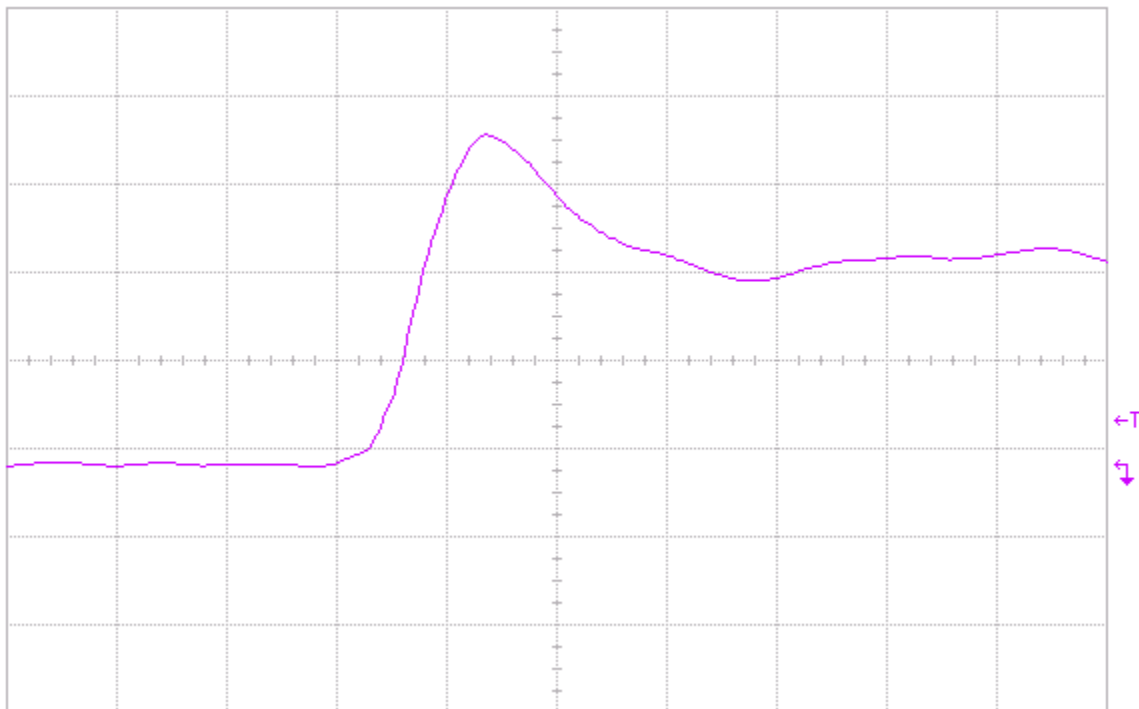


Fig 12(a) Pre-irradiation rising edge of DUT 13615, abscissa scale is 2 V/div and ordinate scale is 2 ns/div.

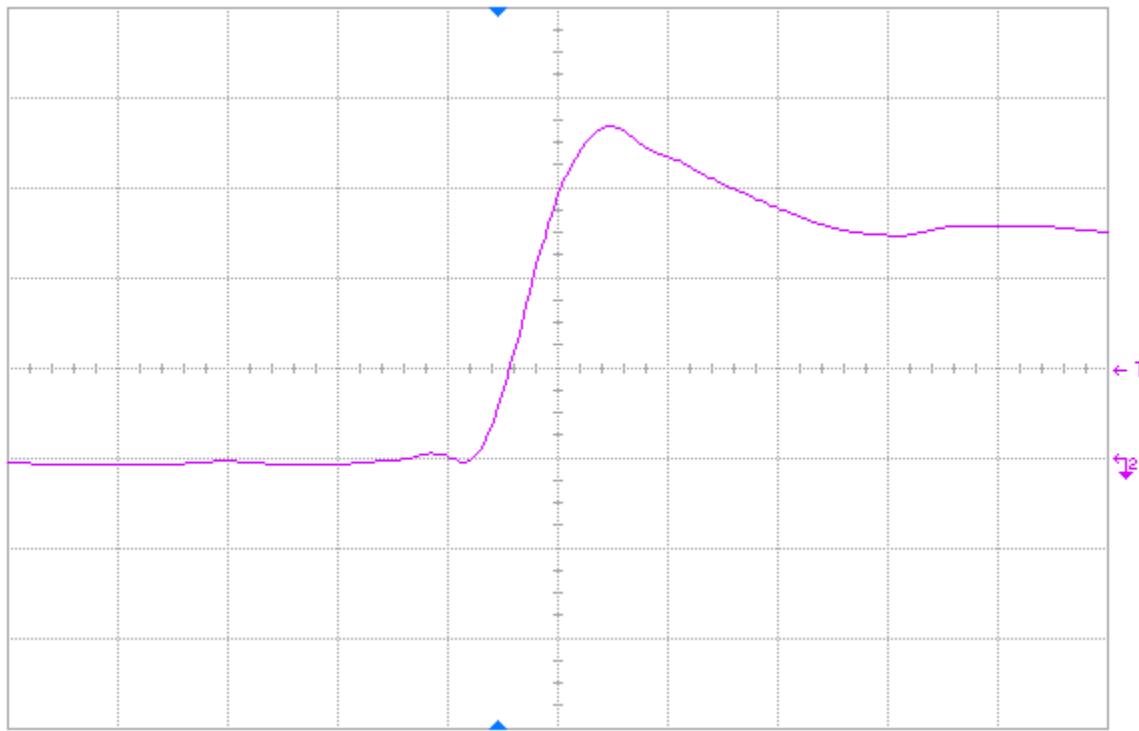


Fig 12(b) Post-annealing rising edge of DUT 13615, abscissa scale is 2 V/div and ordinate scale is 2 ns/div.

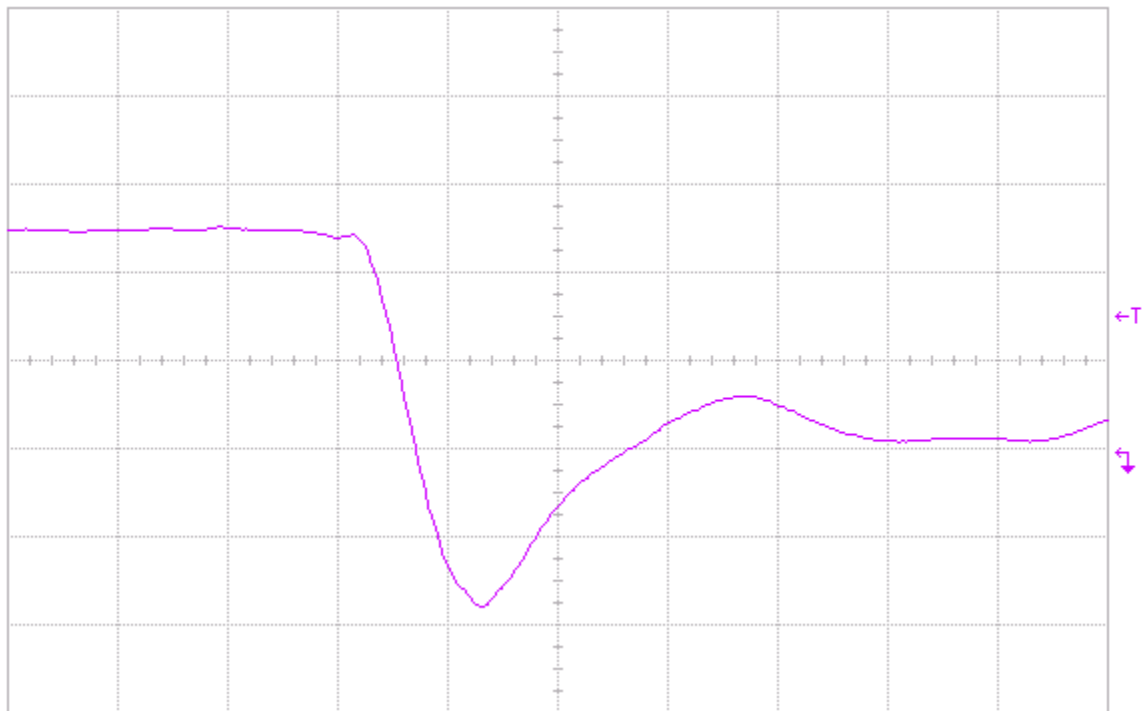


Fig 13(a) Pre-irradiation falling edge of DUT 13503, abscissa scale is 2 V/div and ordinate scale is 2 ns/div.

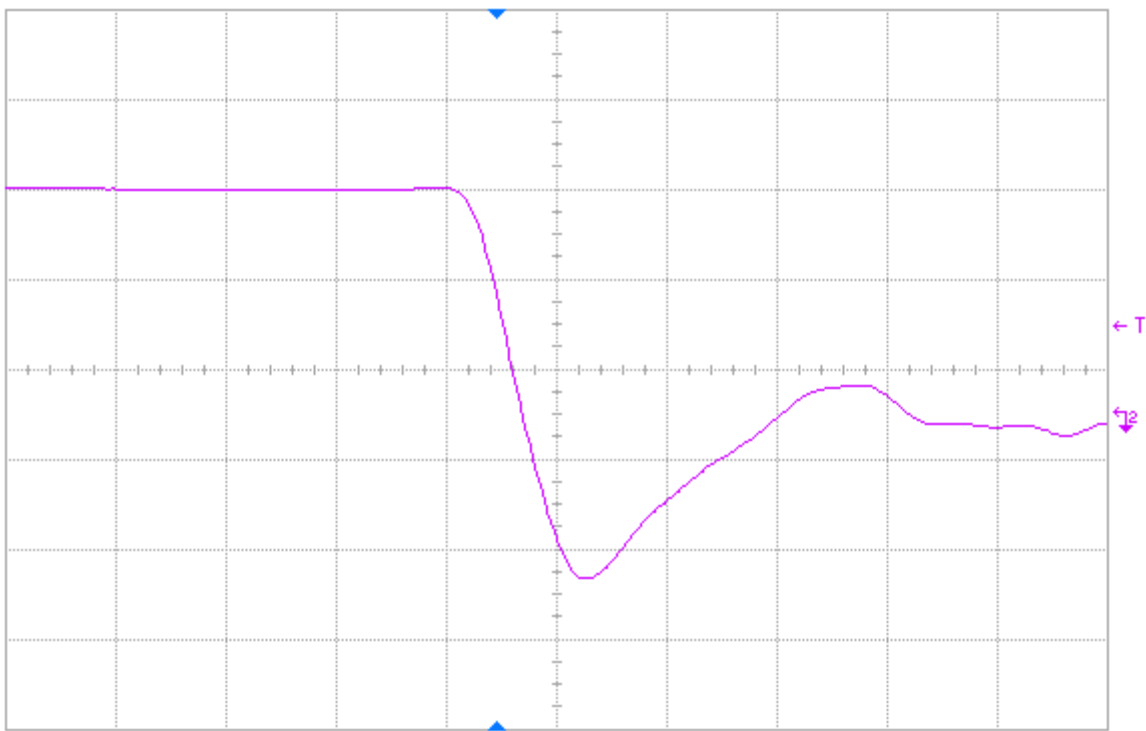


Fig 13(b) Post-annealing falling edge of DUT 13503, abscissa scale is 2 V/div and ordinate scale is 2 ns/div.

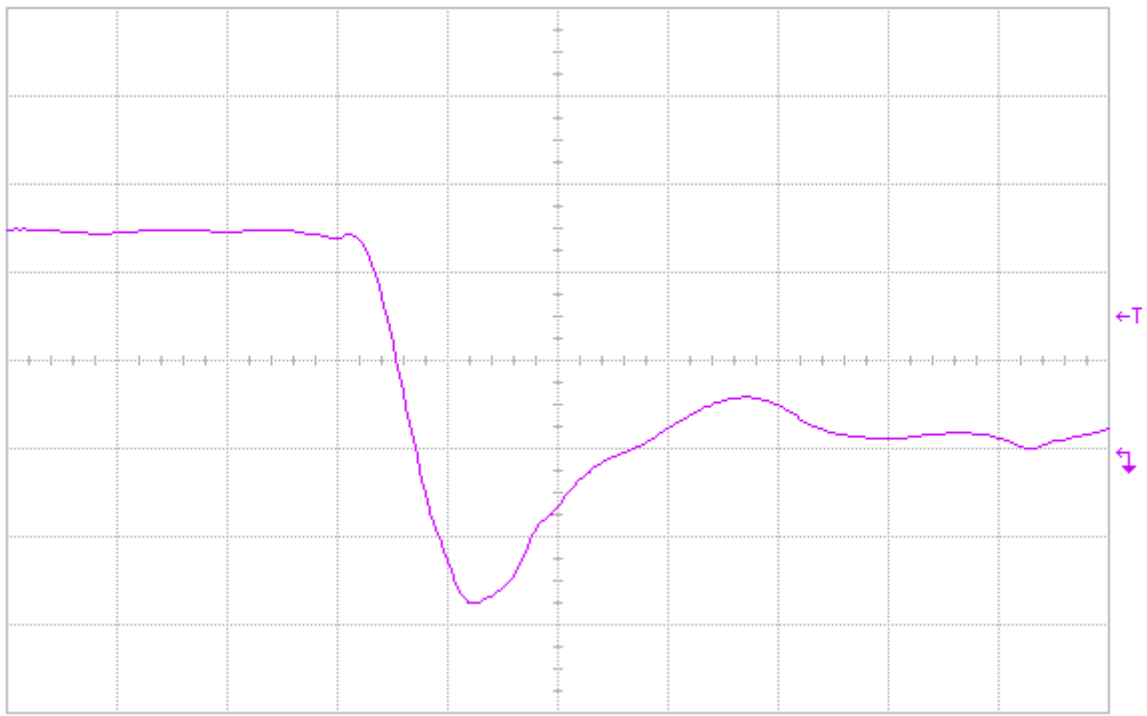


Fig 14(a) Pre-irradiation falling edge of DUT 13529, abscissa scale is 2 V/div and ordinate scale is 2 ns/div.

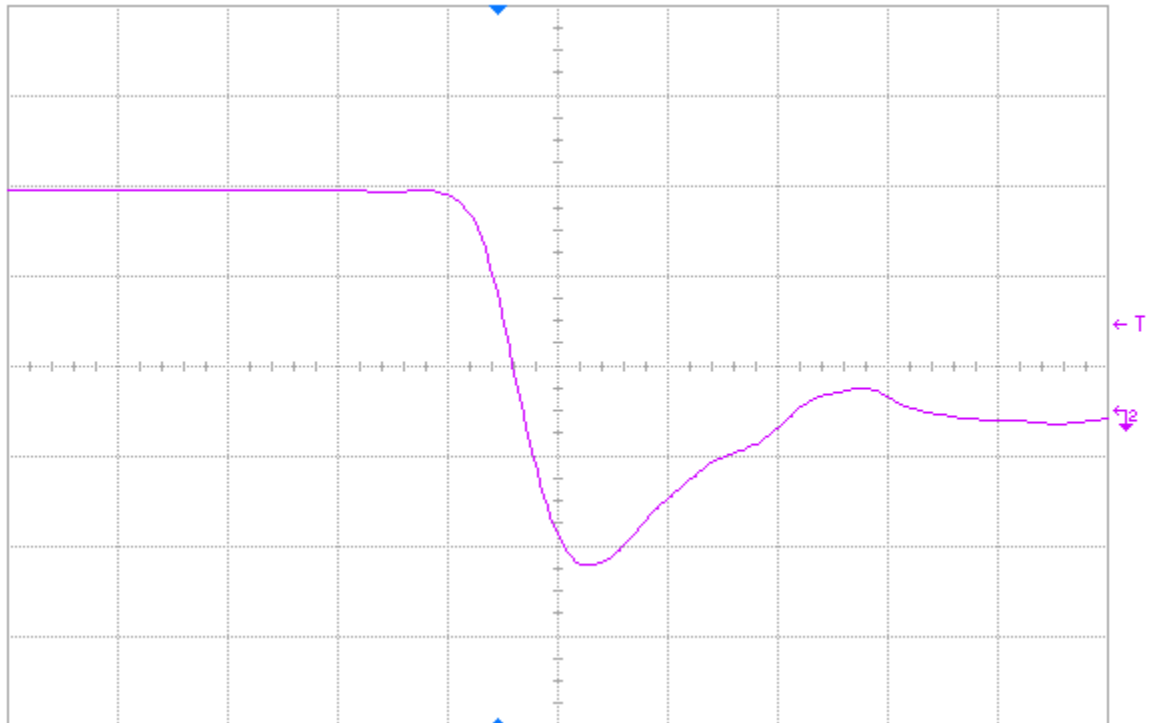


Fig 14(b) Post-annealing falling edge of DUT 13529, abscissa scale is 2 V/div and ordinate scale is 2 ns/div.

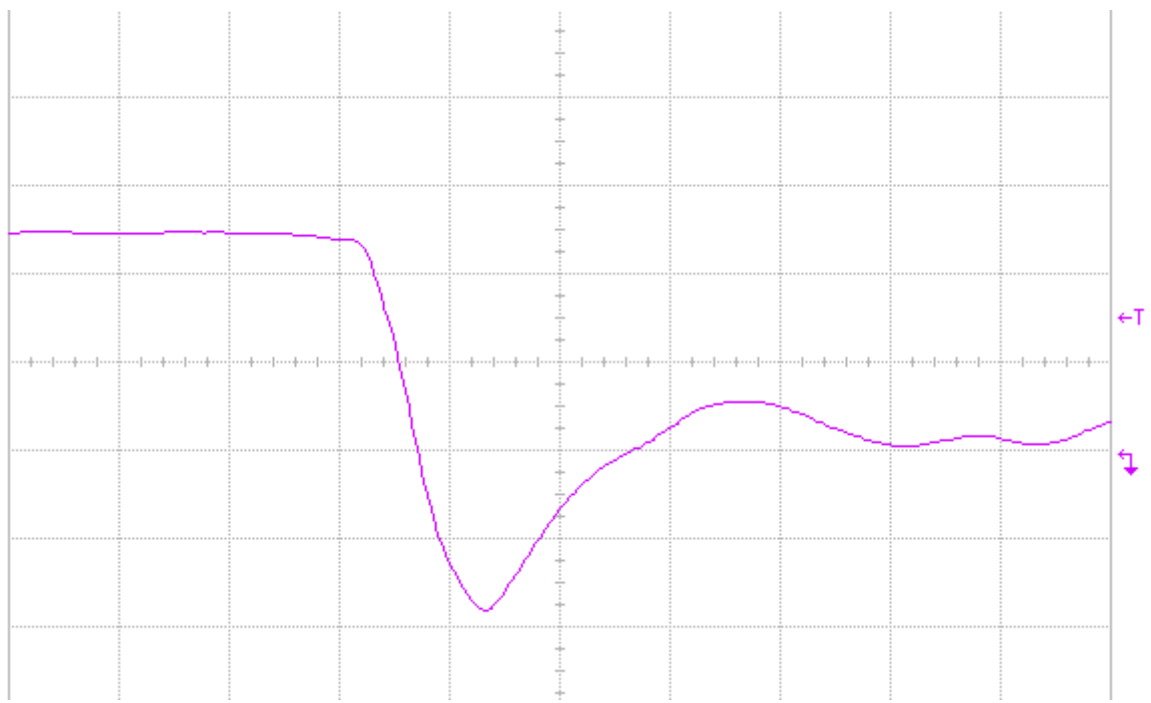


Fig 15(a) Pre-irradiation falling edge of DUT 13545, abscissa scale is 2 V/div and ordinate scale is 2 ns/div.

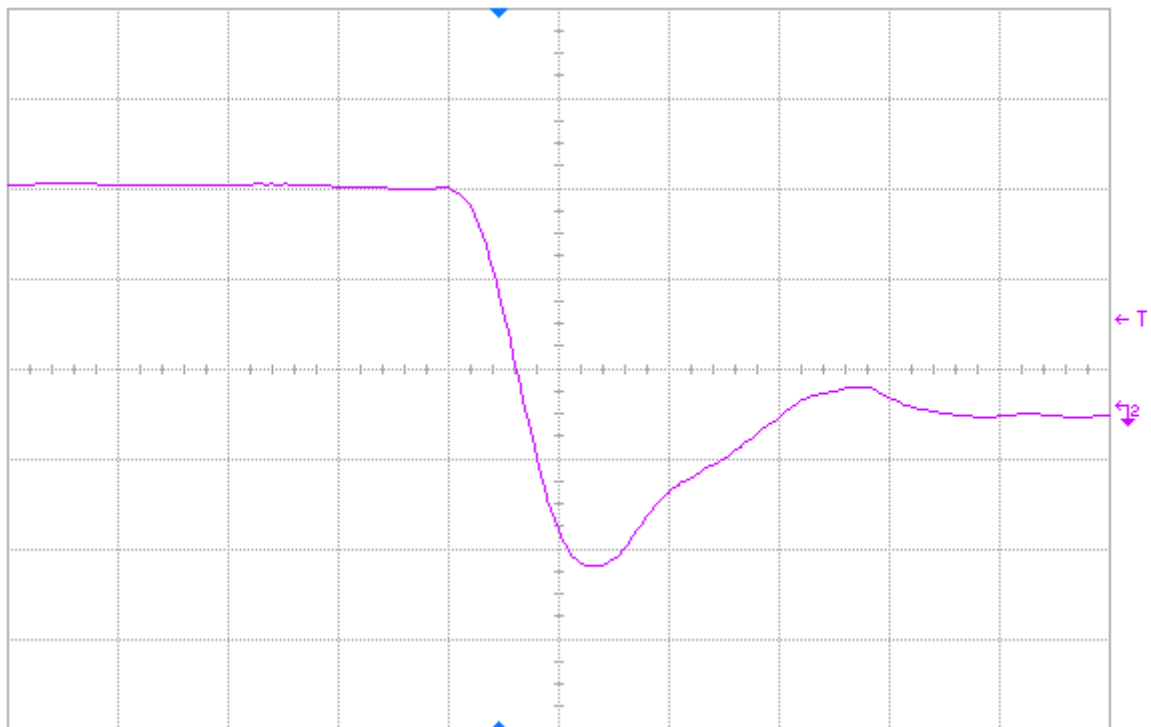


Fig 15(b) Post-annealing falling edge of DUT 13545, abscissa scale is 2 V/div and ordinate scale is 2 ns/div.

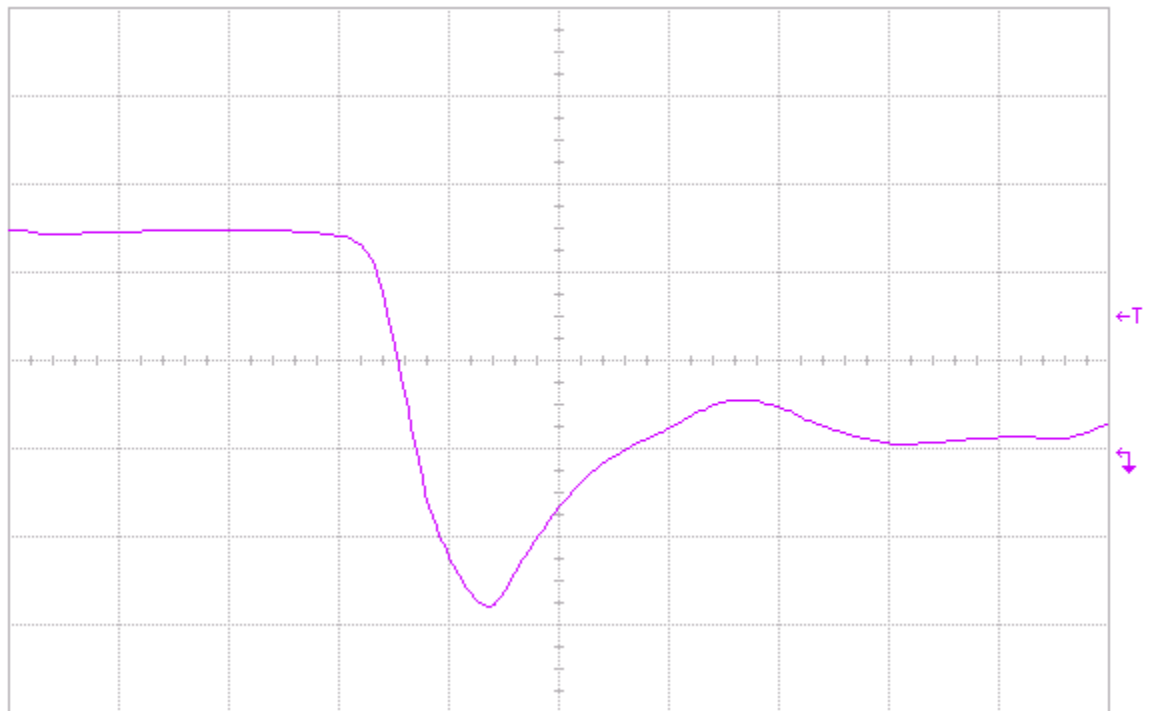


Fig 16(a) Pre-irradiation falling edge of DUT 13611, abscissa scale is 2 V/div and ordinate scale is 2 ns/div.

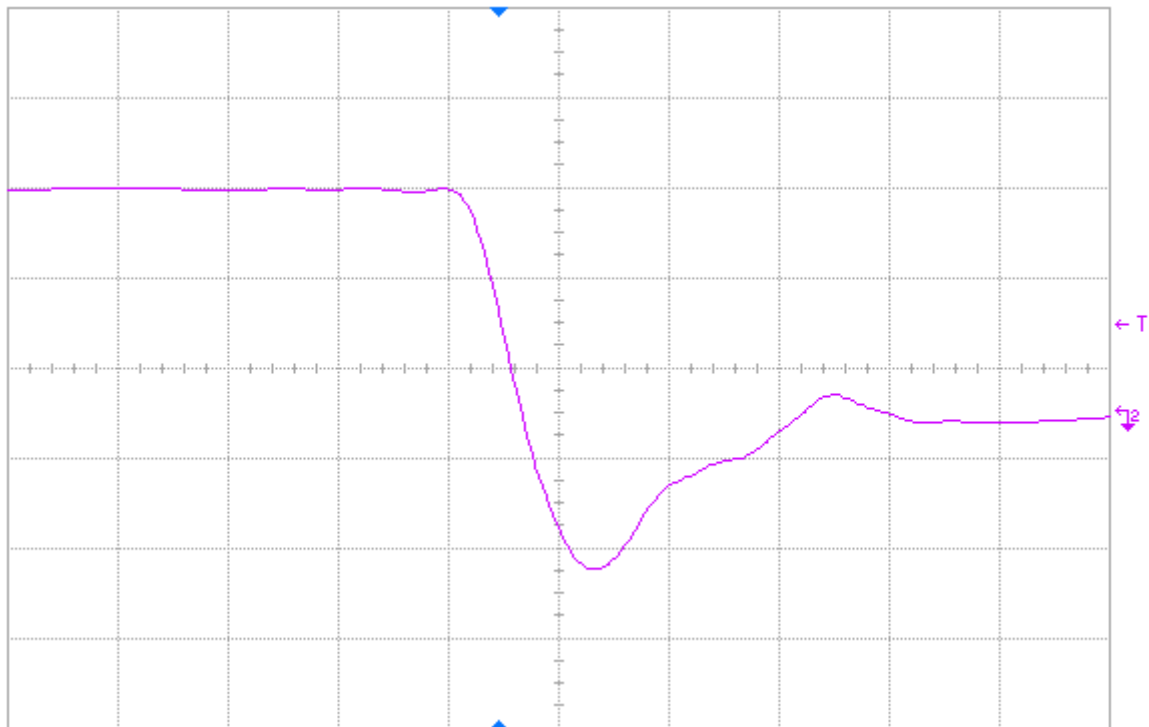


Fig 16(b) Post-annealing falling edge of DUT 13611, abscissa scale is 2 V/div and ordinate scale is 2 ns/div.

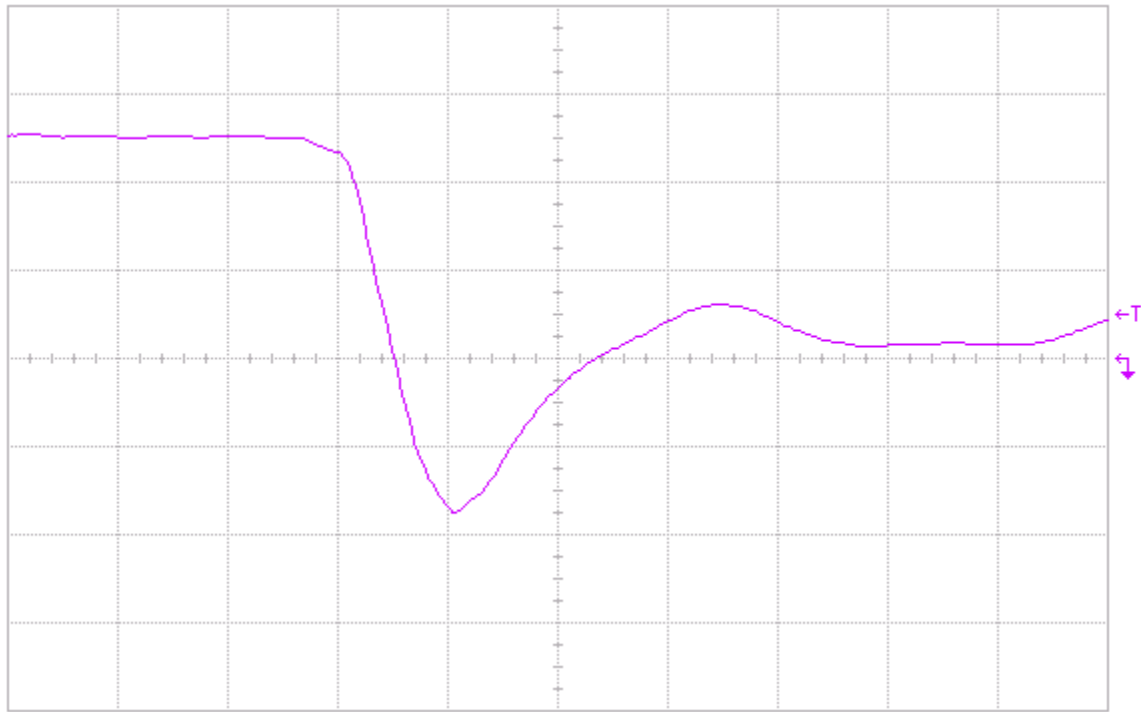


Fig 17(a) Pre-irradiation falling edge of DUT 13615, abscissa scale is 2 V/div and ordinate scale is 2 ns/div.

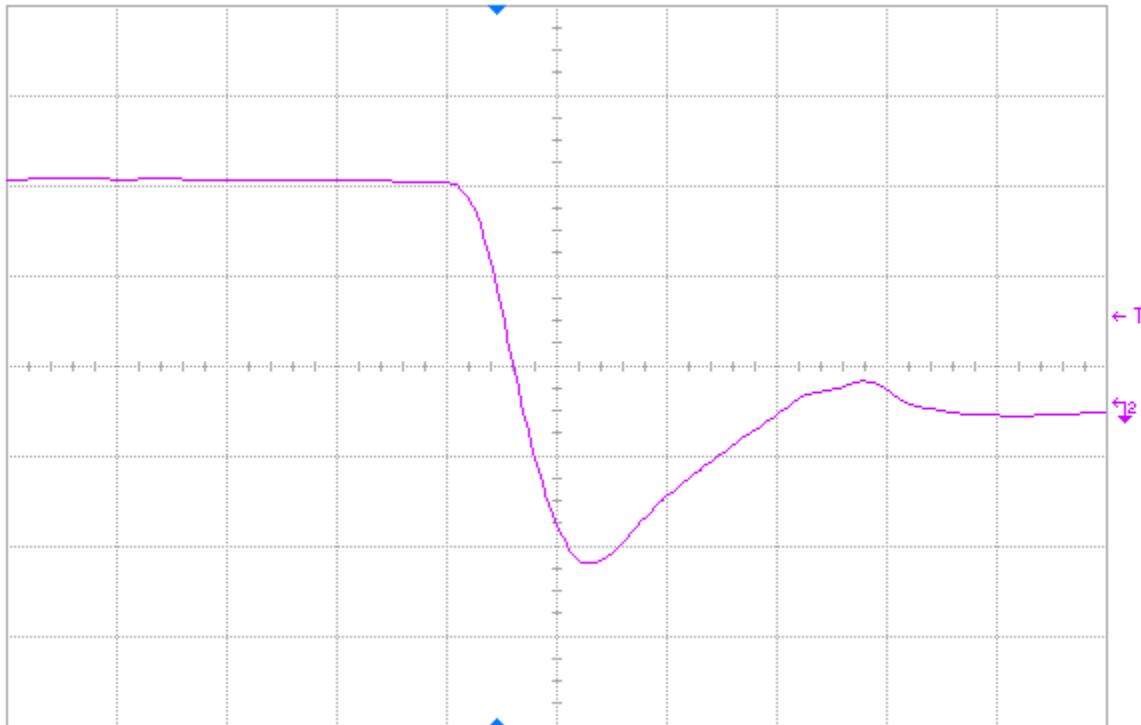


Fig 17(b) Post-annealing falling edge of DUT 13615, abscissa scale is 2 V/div and ordinate scale is 2 ns/div.

APPENDIX A DUT DESIGN SCHEMATICS

